www.sciencemag.org/cgi/content/full/science.aan8895/DC1

Supplementary Material for

Measurement of the neutron lifetime using a magneto-gravitational trap and in situ detection

R. W. Pattie Jr., N. B. Callahan, C. Cude-Woods, E. R. Adamek, L. J. Broussard, S. M. Clayton, S. A. Currie, E. B. Dees, X. Ding, E. M. Engel, D. E. Fellers, W. Fox, P. Geltenbort, K. P. Hickerson, M. A. Hoffbauer, A. T. Holley, A. Komives, C.-Y. Liu, S. W. T. MacDonald, M. Makela, C. L. Morris, J. D. Ortiz, J. Ramsey, D. J. Salvat, A. Saunders,* S. J. Seestrom, E. I. Sharapov, S. K. Sjue, Z. Tang, J. Vanderwerp, B. Vogelaar, P. L. Walstrom, Z. Wang, W. Wei, H. L. Weaver, J. W. Wexler, T. L. Womack, A. R. Young, B. A. Zeck

*Corresponding author. Email: asaunders@lanl.gov

Published 6 May 2018 as *Science* First Release
DOI: 10.1126/science.aan8895

This PDF file includes:

Supplementary Text
Figs. S1 to S9

Other Supplementary Material for this manuscript includes the following:
(available at www.sciencemag.org/content/science.aan8895/DC1)

Data File S1 as a separate .zip file

Table of contents:

Supplementary Text

Section S1: Raw count rates and background and dead time corrections

After being held in the magnetic storage volume for different periods of time, the surviving ultracold neutrons were counted by an in-situ detector described in the main text. The two-sided detector, consisting of a neutron-absorbing boron layer above a ZnS:Ag scintillator above a PMMA light guide connected via wavelength-shifting fibers to a pair of photomultiplier tubes (PMTs), generated for each neutron absorbed a series of individual photons detected by the PMTs, which were then individually counted by a multi-channel scaler. This raw data stream, consisting of a series of individual photon arrival times, was then processed to arrive at a signal that was proportional to the number of neutrons absorbed by correcting for dead time in the system and by subtracting background rates. Two different algorithms were used to process the raw data: one in which a coincidence was required between photon hits in the two PMTs and one in which each photon hit was considered as a separate single event.

In Figure S1, the red and blue histograms show the event count rate in the dagger detector for single PMT triggers and the above threshold two PMT coincidence event respectively. The filling (a), cleaning (b), holding (c), and unloading (d) run segments are shown on the time line and described in the text. The background rate subtracted from the unloading period is estimated from the mean dagger counting rate during the holding period. Applying the coincidence criteria described in the main text reduces the singles counting background rate from 1023(2) s^{-1} to 0.098(9) s^{-1}. The mean count rates during the unloading peak were 7050(20) s^{-1} and 32.8(9) s^{-1} for the singles and coincidence counting methods. The background is then 14.5(1)% and 0.30(4)% of the singles and coincidence unloading peak signal, respectively. The dead time (t_D) was accumulated for each pulse in 1 s wide bins. Each bin in counting time spectrum was divided by the livetime (1-t_D) to correct for t_D. For the coincidence counting, the t_D was computed as a running time that included the time of the first photon to the last photon in the coincidence. For the single photon counting algorithm, a constant t_D=10 ns was used for each photon, determined by measuring individual discriminator pulses.

Section S2: Normalization process

To extract the neutron lifetime from a pair of counts of stored neutrons after different storage times, a relative normalization signal proportional to the number of neutrons loaded into the

storage volume was needed. The UCNτ experiment's primary normalization signal came from an elevated neutron detector, shown in Figure 1, which could only be reached by neutrons with sufficient energy to also escape over the lip of the storage volume. Thus, the normalization procedure made use of neutrons that were otherwise not usable in the experiment.

The raw count rate in the elevated normalization monitor is shown in Figure S2 for the filling period of a typical data taking run. The count rate reflects the density of ultracold neutrons in the guides connecting the lifetime apparatus to the source. Over the duration of the filling period the UCN density in the system builds to saturation with a time constant of 19.1(1) s. The 5 s spacing in the proton beam pulse structure creates the rapid variations observed in the monitor's count rate. The normalization parameter is calculated by integrating this spectrum from t=0 s to t=150 s, with the importance of each UCN count exponentially weighted based on the difference of its detection time and the end of the filling period with a time constant of 70 s. This procedure emphasizes the later portion of the filling period for determining the normalization and minimize the impact of variations of the source early in the filling period.

Section S3: Lifetime correction for upscattering of neutrons on residual gas

In order to estimate the rate at which neutrons are scattered out of the trap by collisions with gas molecules, the UCNτ apparatus includes a pair of cold cathode (CC) gauges to measure the total pressure in the trap as well as a residual gas analyzer (RGA) to assess the composition of the residual gas. The RGA ionizes (and sometimes fragments) gas molecules and then filters the resulting ions by mass, thus providing a qualitative measure of the relative abundances of gas species in the trap. Figure S3 shows the results of a typical RGA scan taken during a data acquisition period.

The dominant residual gas loads are water, nitrogen, and oxygen, all of which have small neutron scattering cross sections compared to complex hydrocarbons, e.g., and of these only water has a cross section large enough to significantly affect the measurement of the neutron lifetime. The presence of water is attributable in part to outgassing from various plastic assemblies, but it is primarily due to desorption from the large internal surface area of the apparatus. Nitrogen and oxygen come from leakage of air or pure nitrogen through various vacuum seals. The remaining peaks are fragments of these species (e.g. OH produced from water at 17 amu) or trace gasses present in negligible quantities. The residual gas composition did not vary significantly during the running period, aside from the gradually decreasing prevalence of water as it was pumped away over the course of approximately a week.

Figure S4 shows the total gas pressure in the storage volume as measured using two cold cathode gauges (CC), averaged over the holding time in each run. The cold cathode gauges were mounted just above either side of the midplane of the storage volume. The North CC gauge was adjacent to a small turbo pump, but the two gauges were roughly equidistant from the main cryopumps. The pattern of pressure dropping over time seen in the plot was caused by the gradual desorption of water after each time the system was opened to make hardware

changes. The correction for gas upscattering stated in the paper was obtained by inspection of the total pressure and estimate of the water fraction across all datasets.

Figure S5 shows the measured gas pressure in the storage volume, averaged between the North and South cold cathode (CC) gauges for the duration of a pair of data runs. A short holding time run is followed by a long holding time run. The trap pressure is quite stable during the course of a typical run, but there are minor variations due to the movement of the various actuators. These variations in pressure can be transient or discrete steps, but typically do not depart from the long term average by more than a few percent. In this example, the variations were caused by increased N2 leakage during motion of the trap door that closed off the storage volume's entrance. No such excursions were observed during the holding periods.

Section S4: Effect of holding field strength on lifetime result

The experiment included a polarization-holding magnet field, perpendicular to the magnetic fields of the permanent magnets which formed the walls of the storage volume, which was designed to eliminate losses of neutrons form the storage volume caused by spontaneous depolarization of the neutrons during the storage time. Any neutron which did depolarize would be attracted instead of repelled by the magnetic wall of the storage volume, and thus rapidly be lost to the experiment, resulting in an artificially short reported neutron lifetime. In order to confirm that the holding field was sufficiently strong to really eliminate unwanted neutron depolarization, we made separate measurements of the lifetime with the field set to different values, and made sure the extracted lifetime did not change significantly.

The lower panel of Figure S6 shows data taken as a function of polarization holding field (solid circles), the measured lifetime at 6.8 mT (dashed line), and a fit to power law model described in the text (solid line). The upper panel shows the difference between the measured blinded lifetime at a given holding field and that at the maximum field of B_0=6.8 mT normalized by the statistical uncertainty of the measurement. The holding field was varied between 0 mT and 6.8 mT and nine measurements of the lifetime were performed with the precision of each measurement between 1.1 s and 13.6 s. The fit to this data down to 0.68 mT yielded a depolarization loss lifetime of $\tau_{DP} = 1.1 \times 10^7$ s (with one sigma uncertainty bounds of 6.0×10^6 s and 5.5×10^7 s) for an uncertainty on the measured neutron lifetime of 0.07 s.

Section S5: Test of the sensitivity of the neutron detector to very low energy (< 5 neV) neutrons

We needed to confirm the ability of the neutron detector to detect even very low energy (<5 neV) UCNs in order to ensure that it could be used to place a limit on any slow heating of neutrons while they were held in the storage volume. We therefore performed some tests in a configuration in which the detector was only exposed to the lowest energy neutrons. In order to do this, we loaded the storage volume as in a standard data acquisition run, but with both cleaners and the detector in their raised position, 43 cm from the bottom of the storage volume. For these runs, both cleaners were kept in their raised position for the entire run, but

the detector was lowered to its first counting position (38 cm from the bottom of the storage volume) after a 20 s holding period. Figure S7 shows the time distribution of UCNs reaching the active cleaner in its raised position. After a 150 s filling period, the trap door is closed, and neutrons with sufficient energy to reach the cleaners are quickly removed from the trap, mostly by the large area main cleaner. A brief pulse of heated neutrons is observed at 154 s, caused by acceleration of some neutrons by the closing of the trap door. By 160 s, the observed counting rate in the active cleaner returns to its background level. These active cleaner results indicated that during the bulk of these "raised cleaner" runs, there were no neutrons remaining in the storage volume with energy sufficient to reach the cleaners at 43 cm; therefore, any neutrons detected in the detector at a height of 38 cm would have very low remaining kinetic energy, of 5 neV or less.

Having shown that in this run configuration the detector was exposed to only the lowest energy neutrons, below 5 neV kinetic energy, we then needed to confirm that the neutron detector was capable of detecting those neutrons. Figure S8 shows the time distribution of these low energy UCNs reaching the detector in this configuration in black. During the 150 s filling period, a large number (off the scale of the plot) of higher energy UCNs reach the detector even in its raised (43 cm) position. At 150 s, the trap door is closed, causing an immediate reduction in the number of detected neutrons, as the ones capable of reaching 43 cm are quickly removed from the storage volume by the cleaners. At 154 s, a small peak of neutrons heated by the closing trap door is observed. At 170 s, the dagger is lowered to its highest counting position, 38 cm from the bottom of the storage volume. UCNs that can reach 38 cm but avoid the cleaning height at 43 cm have kinetic energies below 5 neV when impacting the detector. Figure S8 demonstrates the ability of the detector to count these neutrons, removing them from the storage volume with a characteristic time of 260 s. Figure S8 also shows in orange a curve with a 260 s decay time fitted to the detected neutrons.

Section S6: Limitation on effect of evolution in phase space of the stored neutron population

One possible systematic effect in this experiment is that caused by phase space evolution, or an effective variation of total detector efficiency as a function of the time the neutrons are held in the storage volume. One might conjecture, for example, that the neutrons as loaded in the storage volume occupy phase space that is easily accessible to the detector located at the mid-plane of the storage volume, but over time migrate to regions of phase space that are less accessible to the detector. This effect would cause an effective change in efficiency of the detector between the long and short holding time runs and thus affect the reported lifetime. If this effect were present, it would also cause a change in the effective time needed to collect the neutrons in each counting period, thus changing the centroid of the time distribution of counted neutrons relative to the nominal start of the counting time. Therefore, we could put a limit on this systematic effect by calculating the uncertainty in the centroid of the detected neutron distribution. The nine step counting procedure was most sensitive to this possible effect, and therefore we performed this calculation on that run condition to get the most

conservative limit on this effect. The centroid of the coincidence detection curve from Figure S9, which shows the detection curves for the sum of all short and long holding time runs from run condition C in red and blue respectively, was used for this calculation, applying the standard formula:

$$\sigma_{\bar{x}} = {}^{\sigma_x}\!/_{\sqrt{N}} = {}^{1}\!/_{\sqrt{N}} \sqrt{{}^{\sum_{bins} N_i \, t_i^2}\!/_{(\sum_{bins} N_i - 1)}}$$

This value, 0.10 s for the nine step long holding time counting distribution, gives an estimate of the limit of the possible effect on the measured life time by phase space evolution.

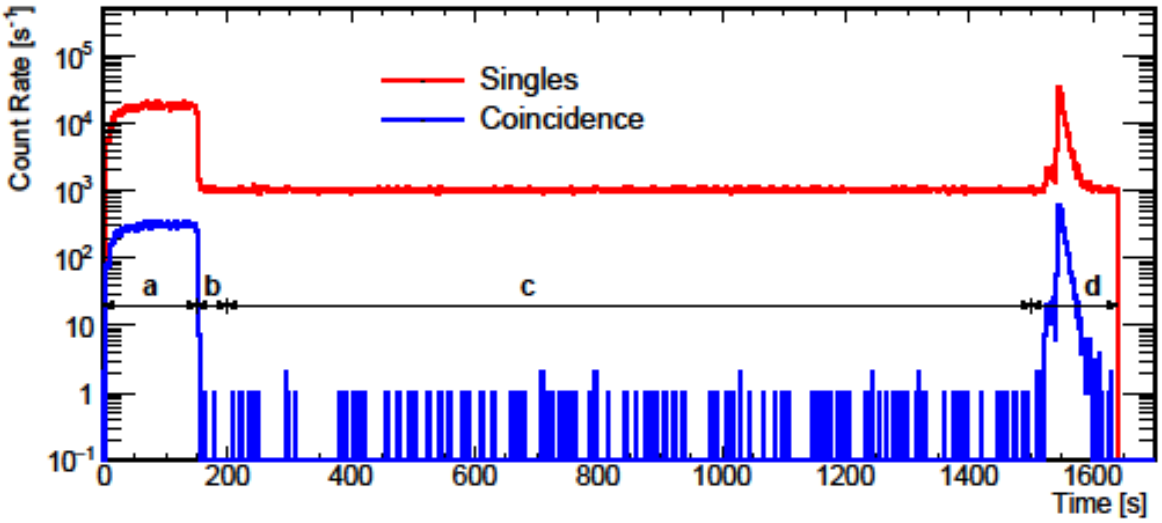

Figure S1: Raw data from a typical data run from Run Condition D: three step unload. The underlying data can be found in the Supplementary Materials in FigureS1.csv.

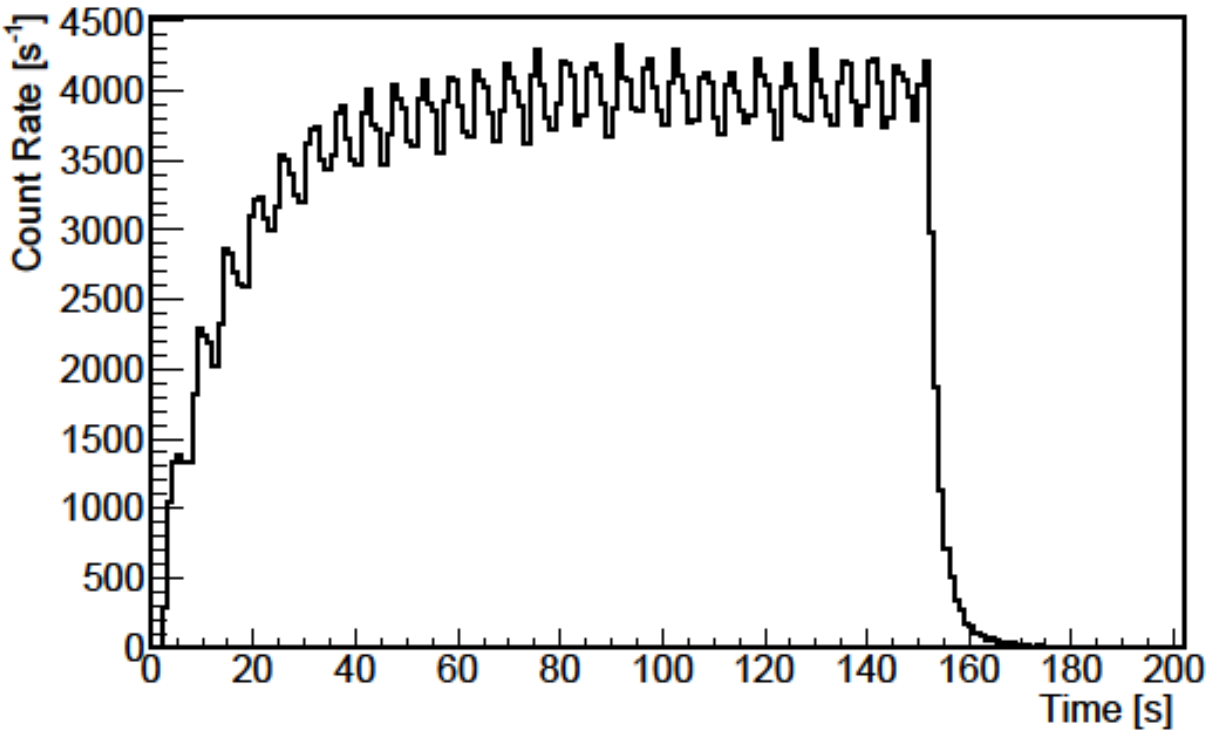

Figure S2: Raw count rate in the elevated normalization monitor for a typical data acquisition run. The underlying data can be found in the Supplementary Materials in FigureS2.csv.

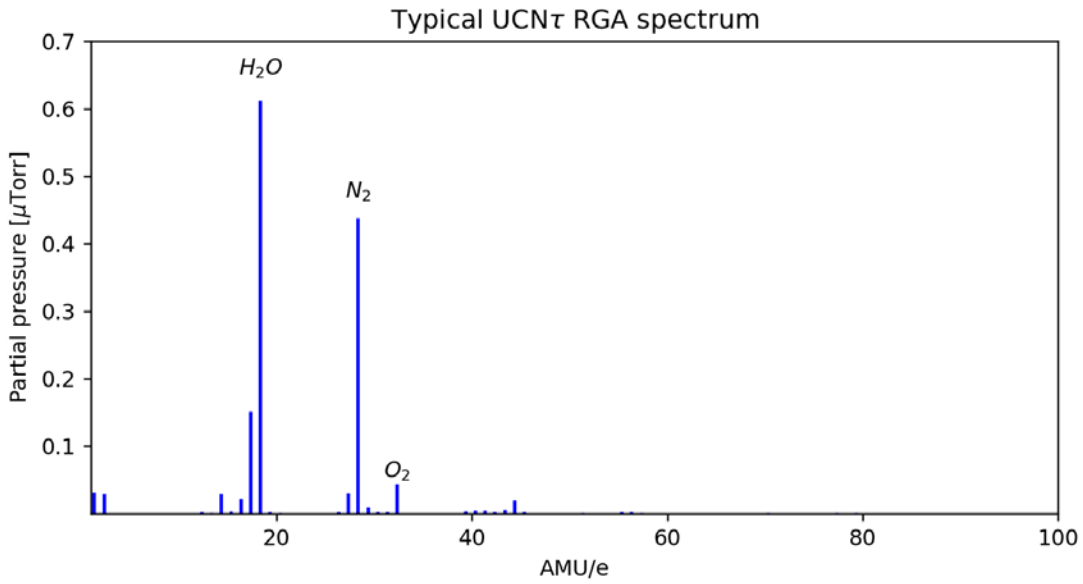

Figure S3: Results of a typical Residual Gas Analyzer scan taken during the data acquisition period. The underlying data can be found in the Supplementary Materials in FigureS3.csv.

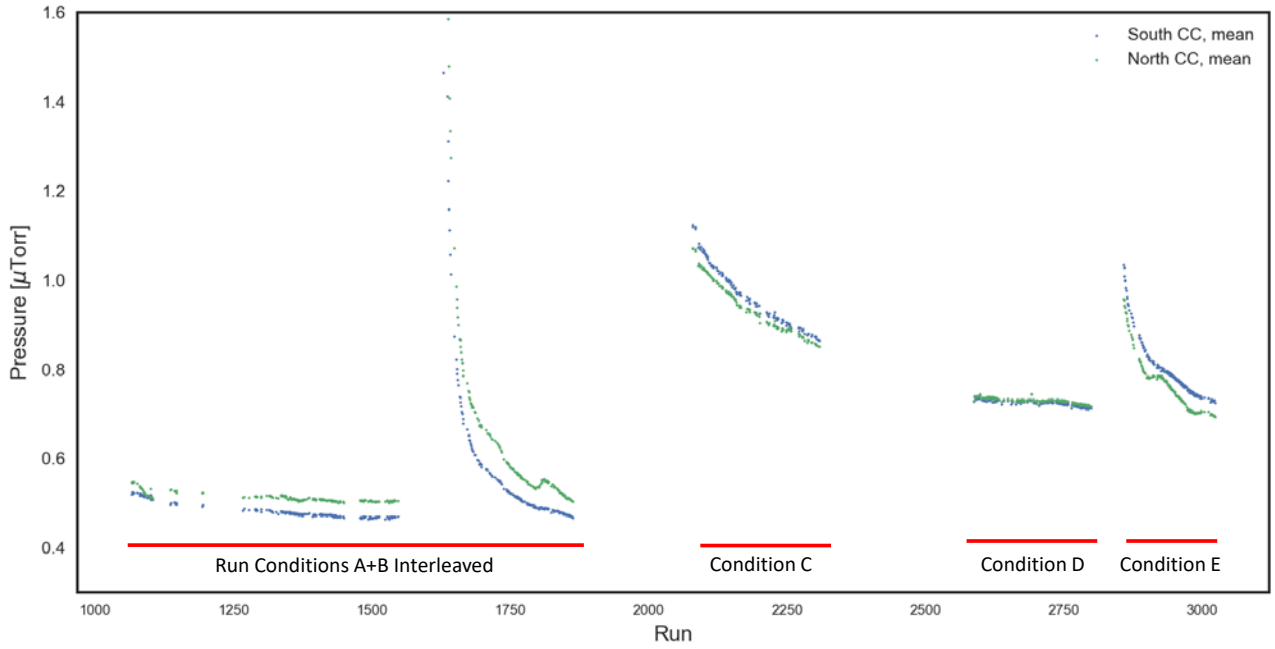

Figure S4: Measured residual gas pressure for the data set reported in this paper. The underlying data can be found in the Supplementary Materials in FigureS4.csv.

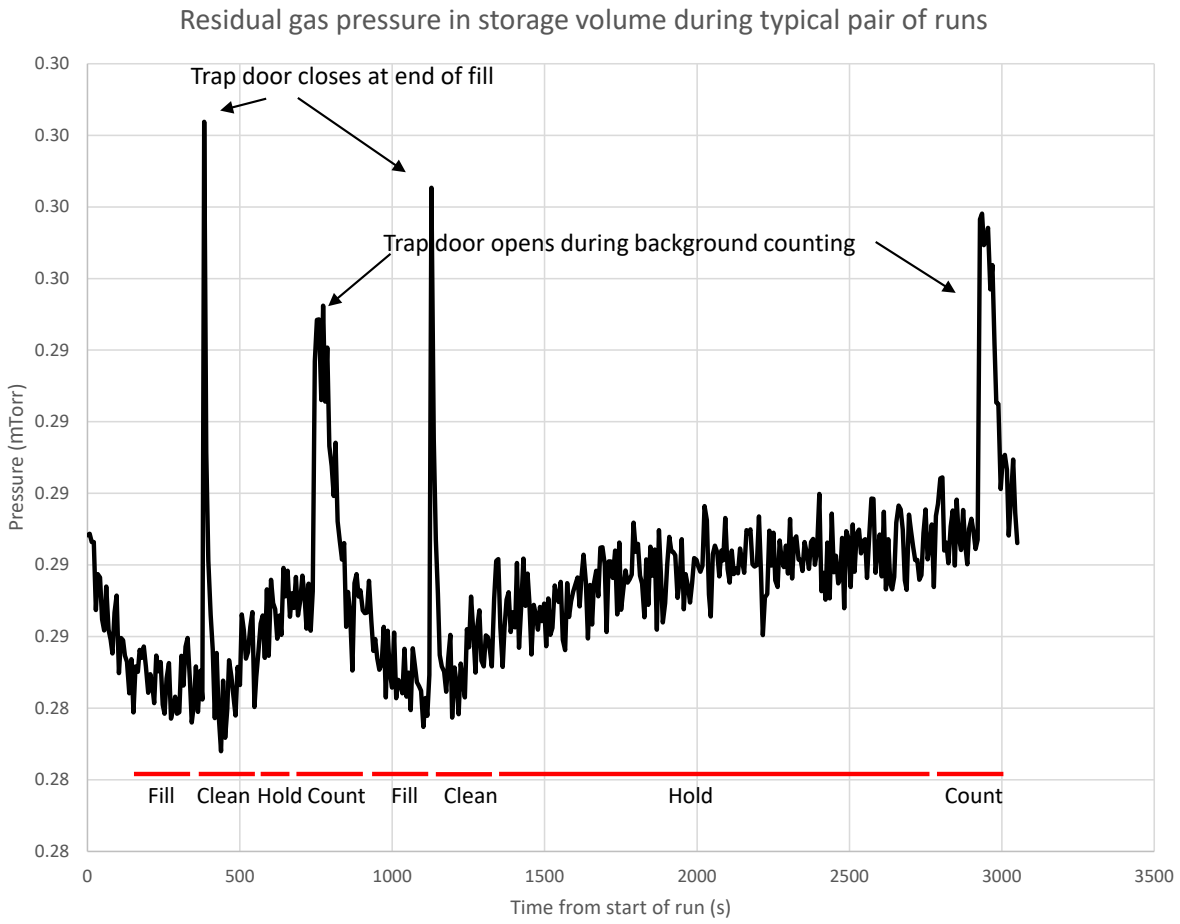

Figure S5: Measured gas pressure during a typical pair of data runs. The underlying data can be found in the Supplementary Materials in FigureS5.csv.

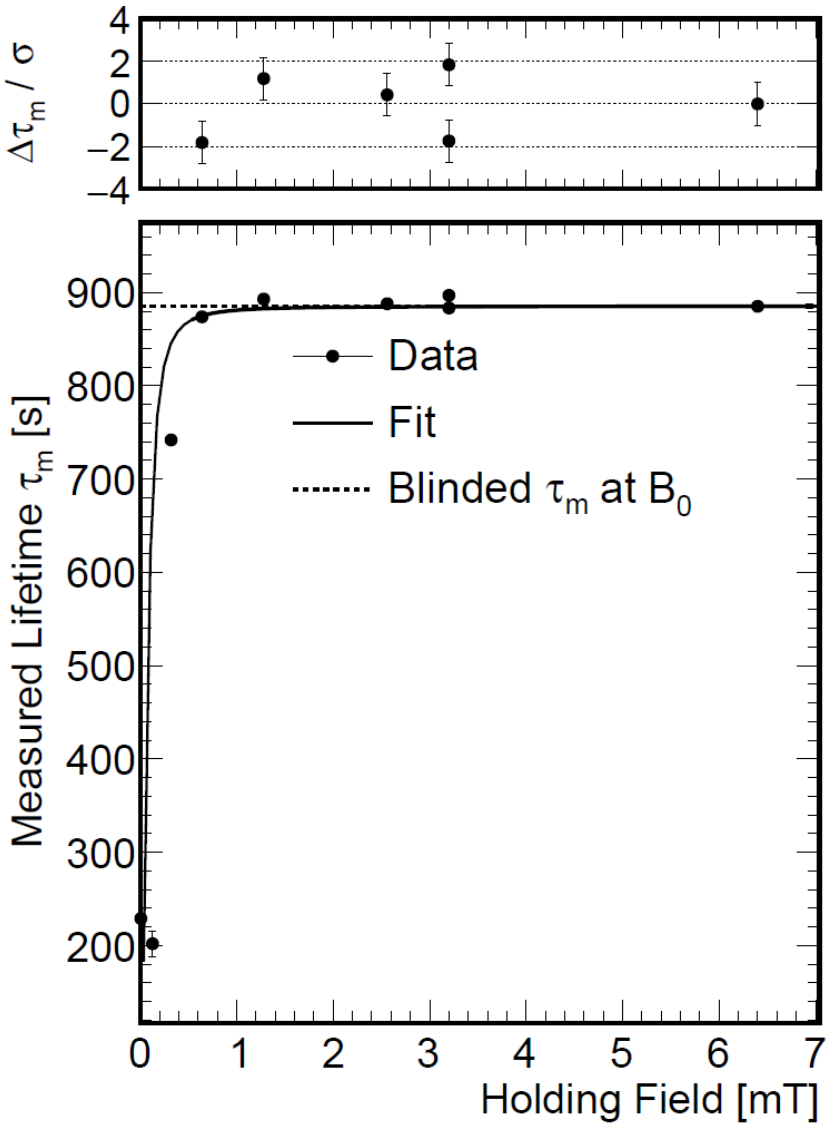

Figure S6: Data taken as a function of polarization holding field, and fit to model. The underlying data can be found in the Supplementary Materials in FigureS6.csv.

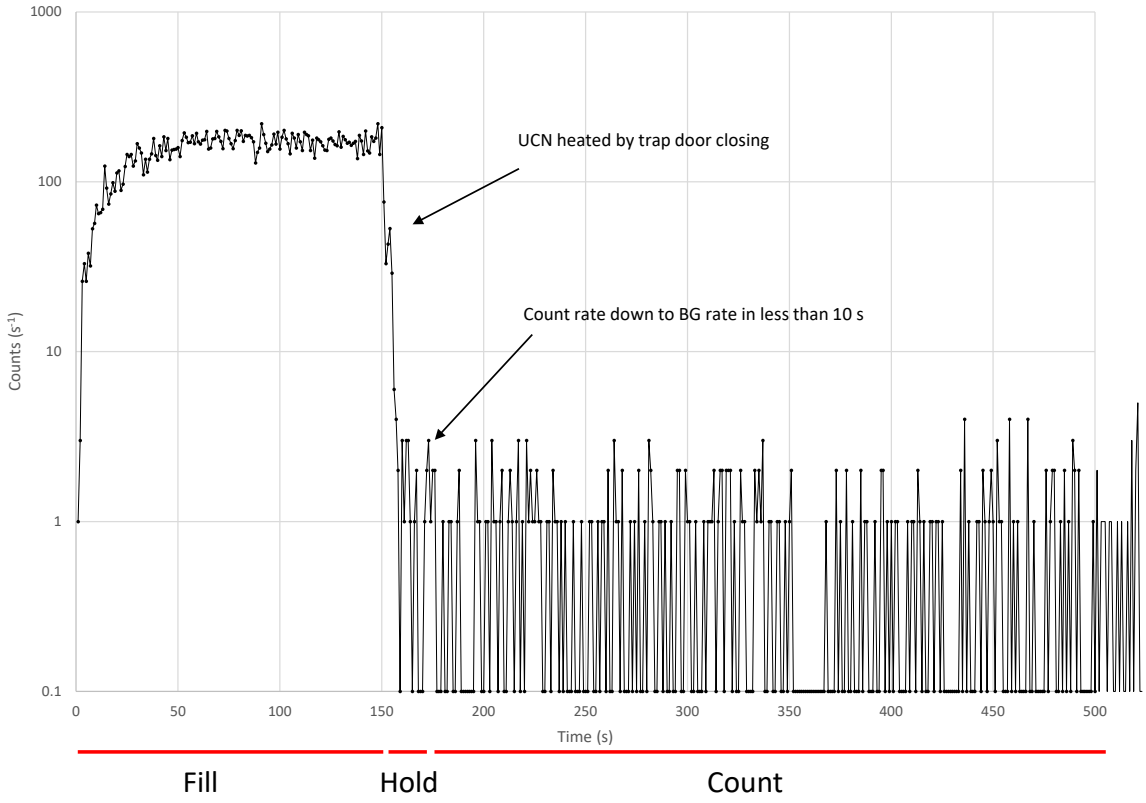

Figure S7: Time distribution of neutrons detected by active cleaner in its raised position. The underlying raw data is included in the Supplementary materials in FigureS7.csv.

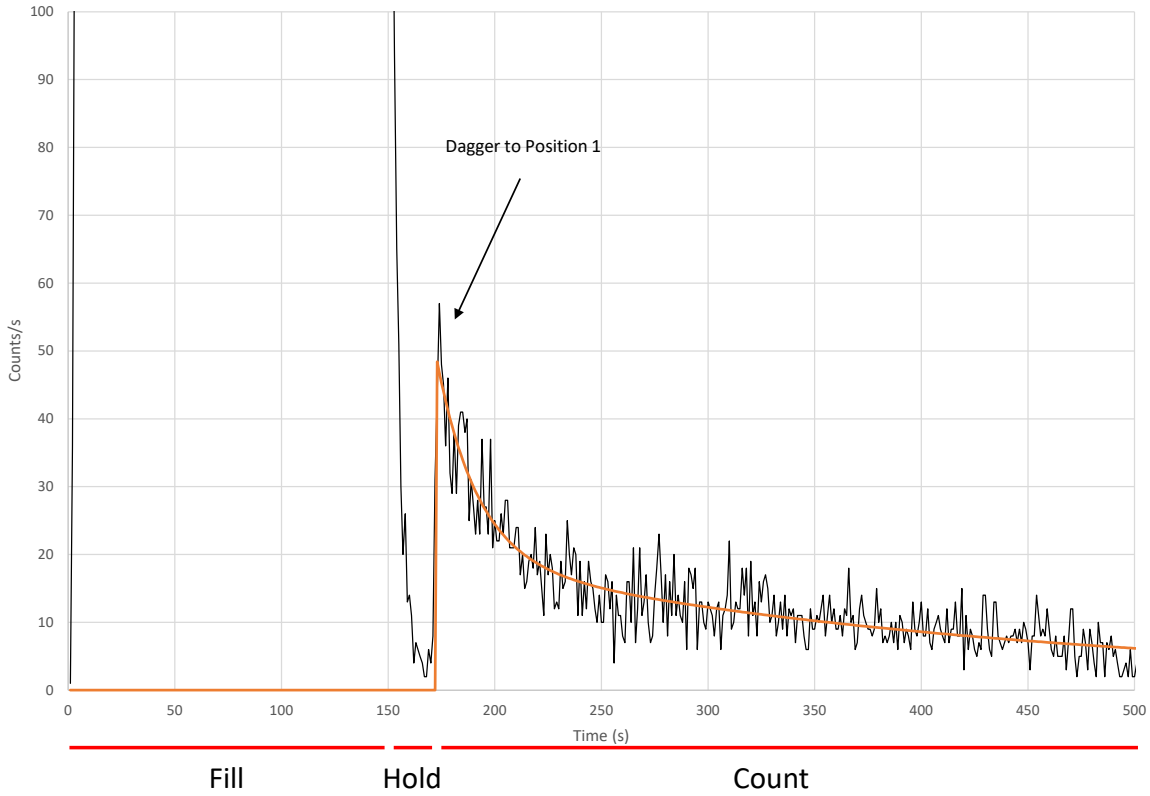

Figure S8: Time distribution of neutrons detected by the detector at its highest counting position, with cleaners raised throughout. The underlying data as well as the fit parameters are included in the supplementary material in FigureS8.csv.

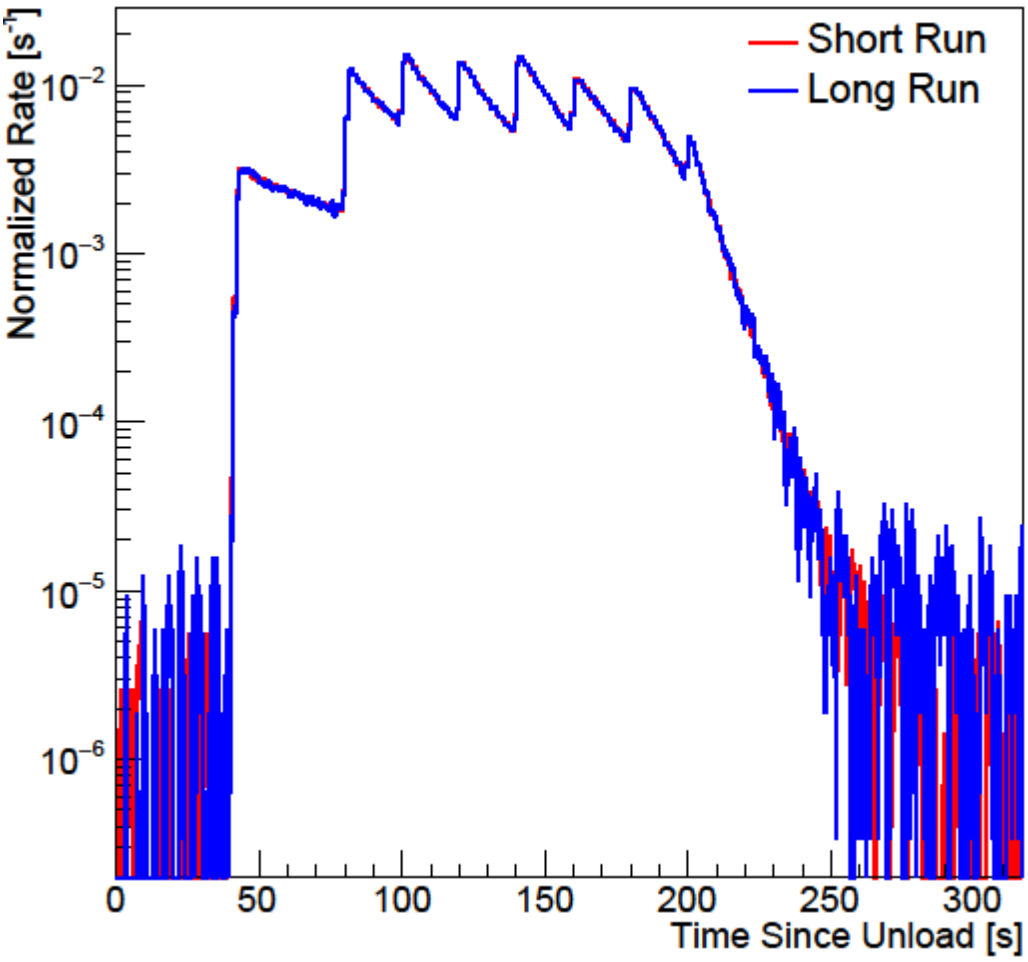

Figure S9: Calculation of uncertainty in centroid of detected neutron time distribution. The underlying data can be found in the Supplementary Material for this paper in FigureS9.csv.